Journal of Cerebral Blood Flow & Metabolism (2011) 31, 1852–1862

www.jcbfm.com

Two-photon fluorescence microscopy study of cerebrovascular dynamics in ultrasound-induced blood–brain barrier opening

Eunice E Cho[1], Jelena Drazic[1,2], Milan Ganguly[1], Bojana Stefanovic[1,2] and Kullervo Hynynen[1,2]

[1]*Imaging Research, Sunnybrook Research Institute, Toronto, Ontario, Canada;* [2]*Department of Medical Biophysics, University of Toronto, Toronto, Ontario, Canada*

Blood–brain barrier (BBB) disruption can be achieved with ultrasound (US) and circulating microbubble (MB) contrast agent. Using dorsal US sonication and Definity, an MB contrast agent, responses of the cortical cerebral vasculature to BBB opening were observed with varying acoustic peak negative pressure (0.071 to 0.25 MPa) under two-photon microscope. Wistar rats with a craniotomy were sonicated with a single piezoelectric transducer following the intravenous injection of Texas Red for visualization of vasculature and leakage from BBB opening. Based on time-dependent intensity change in the extravascular area, the leakage was classified into three types: fast, sustained, and slow. Fast leakage was characterized by a rapid increase to peak intensity during sonication, but a decrease afterwards, occurring at all pressures and vessels sizes analyzed in our study. Sustained leakage was indicated by a similar, immediate increase to peak intensity but one that remained elevated for the duration of imaging, occurring at low-to-intermediate pressures. Slow leakage began 5 to 15 minutes after sonication, dominating at low pressures, and was more prevalent among smaller vessels than fast and sustained leakage. Our study showed the possibility of controlling leakage type and vessel size in US-induced BBB opening through varying acoustic pressure.
Journal of Cerebral Blood Flow & Metabolism (2011) **31,** 1852–1862; doi:10.1038/jcbfm.2011.59; published online 20 April 2011

Keywords: blood–brain barrier; brain imaging; two-photon microscopy; ultrasound; vasospasm

Introduction

Cerebral capillaries have specific properties that contribute to the formation of the blood–brain barrier (BBB). In the brain, the endothelial cells (ECs) have continuous tight junctions that differ from systemic ECs (Toole, 1990). In addition, brain ECs have a high number of mitochondria (Oldendorf *et al*, 1977), a lack of fenestrations (Fenstermacher and Kaye, 1988), and reduced pinocytosis (Sedlakova *et al*, 1999). Membrane proteins, astrocytes, and pericytes act together with the brain ECs to form a BBB that limits molecular diffusion across the capillary wall. This BBB selectively allows substances of certain sizes and polarity, <400 to 500 Da and highly soluble in lipid, to cross between the tissue and the lumen of cerebral blood vessels. Due to this restriction at the cerebral capillary bed, the delivery of currently available drugs and antibody therapies has been limited, posing difficulties in treating central nervous system pathology (Pardridge, 2005). A number of studies have found that ultrasound (US) sonication in combination with microbubble (MB) contrast agents can modify the permeability of the BBB (Hynynen *et al*, 2001, 2005, 2006; McDannold *et al*, 2007, 2008; Yang *et al*, 2007; Raymond *et al*, 2007; Reinhard *et al*, 2006; Choi *et al*, 2007). Electron microscopy analysis of BBB disruption with MB/US treatment has confirmed increased molecular passages across the capillary bed (Sheikov *et al*, 2004). The BBB can be transiently and selectively disrupted at the US focus without acute (Hynynen *et al*, 2001) or chronic neuronal damage (Hynynen *et al*, 2006) or impact on the animal behavior (Howles *et al*, 2010). Transient changes in the BBB permeability open up new windows for noninvasive, targeted drug delivery in the central nervous system (Kinoshita *et al*, 2006*a*, *b*; Raymond *et al*, 2008; Jordao *et al*, 2010).

Correspondence: Dr K Hynynen, Department of Medical Biophysics, Imaging Research, 2075 Bayview Avenue, Room S665B, Toronto, ON, Canada M4N 3M5.
E-mail: khynynen@sri.utoronto.ca
This study was supported by Canadian Research Chairs program and grants from the Terry Fox Foundation and NIH (No. EB003268).
Received 26 January 2011; revised 24 March 2011; accepted 29 March 2011; published online 20 April 2011

Magnetic resonance imaging has been prevalently used in the studies referenced above on the BBB disruption. As a result of large time delays between sequential images, which are in the order of minutes on average for quality images, there are still shortcomings in our understanding of the biophysical mechanism of BBB opening with magnetic resonance imaging studies alone. In addition to analyzing BBB disruption with magnetic resonance imaging, real-time monitoring of the BBB disruption at the level of individual vessels needs further analysis. As opposed to limited spatial resolution of magnetic resonance imaging, two-photon microscopy allows *in vivo* visualization of the cerebral vasculature and neurons at the subcellular level. Unlike other types of fluorescent microscopy that can scan only the peripheral regions, the two-photon microscope is capable of *in vivo* imaging to about 500 to 600 μm in depth (Kleinfeld *et al*, 1998). With longer excitation wavelength and special setup, an imaging depth of 1 mm could even be achieved *in vivo* with two-photon microscope (Kobat *et al*, 2009). Photobleaching and phototoxicity can be minimized with two-photon microscopy even with repeated imaging as two-photon excitation occurs only at the point of focus (Denk *et al*, 1990). The two-photon microscope has served as the principal instrument in our preclinical study as it allows observation of in-depth vascular dynamics.

A previous study on multiphoton imaging of BBB opening assessed cerebrovascular dynamics and the kinetics of dye leakage after US sonication from the ventral side of the brain (Raymond *et al*, 2007). Three leakage processes were identified in this study: hemorrhage, focal disruption, and transcytosis. Frequent vasoconstriction accompanying BBB disruption was also noted. Certain findings from this study that warrant further investigation include constriction duration and its repeatability as well as differences in arterial versus venous leakage. By extending the two-photon analysis of US-induced BBB opening to rats instead of mice, we aimed to confirm the repeatability and robustness of the three leakage mechanisms as well as estimate the timing parameters of these processes. We used dorsal rather than ventral US sonication to minimize tissue attenuation and variations in the US exposure level. We specifically wanted to study effects of different acoustic pressures on BBB disruptions and of vessels of varying sizes. Our aim was to investigate any vessel caliber dependence of the leakage and characterize the kinetics of this process.

Materials and methods

Animal Preparation

A total of 20 male Wistar rats (120 to 200 g) were used in this study. Animals were placed in an induction box and allowed to breathe oxygen-enriched air containing 5% isoflurane. Once fully relaxed, isoflurane was reduced to 2% during the rest of the procedures. Medical air was ventilated to maintain the minimum oxygen saturation of 98%. After tracheotomy, the animal was restrained in a sterotaxic frame using ear bars and a bite bar. Intramuscular injection of glycopyrrolate (20 μg/kg) was also administered every hour to reduce secretion and help with breathing. The animals were connected to a ventilator and were constantly monitored by a pulse oximeter. The body temperature was controlled using electrical heating pad set at 37.5°C. The tail vein was cannulated with a catheter made with a 23-G needle attached to polyethylene tubing and secured with cyanoacrylate glue. A cranial window (5 mm × 5 mm) was prepared on the right side of the skull about 3 mm lateral from the midline by locating the primary somatosensory cortex, about 3 mm posterolateral to bregma. In cases where there was bleeding from removal of the dura, a second window was prepared contralaterally. The cranial window was closed using 1% agarose and a coverslip, secured using dental acrylic cement (K-Dental, Toronto, ON, Canada) and cyanoacrylate glue (Figure 1A). Then, anesthesia was switched to a cocktail of ketamine (100 mg/kg) and xylazine (10 mg/kg) administered through intramuscular injection for US application and imaging. The exposed brain within the cranial window was marked with tissue dye (Sigma-Aldrich, Oakville, ON, Canada) before removal to help identify the sonicated region. After euthanasia, brains were postfixed in 10% neutral buffered formalin followed by routine processing for paraffin wax embedding. Four-micron-thick coronal sections were cut every 150 μm throughout the sonicated region. Sections were subsequently stained with hematoxylin and eosin to identify extravasated red blood cells and other tissue damage. All the procedures have been approved by our institutional Animal Care Committee.

Ultrasound Application

A single-element, ring-shaped piezoelectric transducer (thickness: 1.4 mm, height: 1.19 mm, outer diameter: 10 mm) was manufactured in-house and driven by a function generator (Agilent, Santa Clara, CA, USA) and a 53-dB RF Power Amplifier (NP Technologies Inc, Newbury Park, CA, USA). The applied forward and reflected RF power was monitored during the sonication by a computer via an in-house constructed detector circuit. The computer system controlled the entire sonication process. A 15-mm cover glass was attached to the transducer with cyanoacrylate glue for direct attachment to the rat skull (Figure 1B). The frequency of our transducers varied from 1.15 to 1.2 MHz. Average input electrical powers were in the range of 0.26 to 1.45 W in order to produce varying acoustic pressures. A vibrometer (PSV-400-M2-20 20 MHz; Polytec, Tustin, CA, USA) was used to measure acoustic peak pressure amplitudes at various input electrical powers and gave results in the range of 0.071 to 0.25 MPa in an *ex vivo* experiment with the fiber inserted in a skull with a brain in a setup identical to the experiments. Twenty rats were sonicated for 120 seconds each, using a pulse duration of 10 milliseconds and repetition frequency of 1 Hz

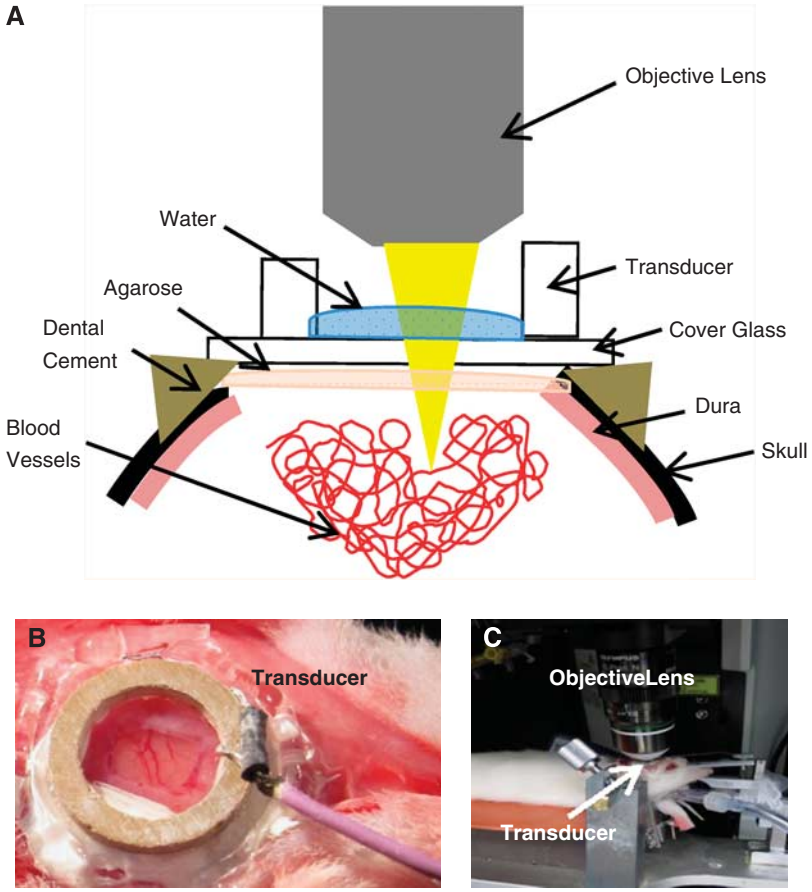

Figure 1 The experimental setup. (**A**) Sagittal view of the entire setup. (**B**) After a craniotomy, the single-element piezoelectric transducer, attached to a glass cover slip, was secured with cyanoacrylate glue and dental cement. The ring transducer also served as water well for water-immersion objective lens. (**C**) Animal is secured on streotaxic stage for two-photon imaging.

(Hynynen *et al*, 2001). Definity (Lantheus Medical Imaging, Billerica, MA, USA) was diluted with saline in 1:10 volume ratio and injected through the tail vein at a final concentration of 0.02 mL/kg. The saline solution of MB was injected either 10 seconds before or after the start of US sonication to observe any difference in MB injection time. Total of eight animals were injected with MB 10 seconds before US sonication and 12 animals were injected with MB 10 seconds after the start of US sonication. Each animal was sonicated once or twice; if no leakage was observed within an hour, sonication was applied up to four times. Control animals were either sonicated without MB injection or injected with MB without any sonication. Two animals were injected with MB alone and two were sonicated at 0.13 MPa without MB injection.

Two-Photon Imaging

After the craniotomy was complete, the stereotaxic frame was moved to the microscope stage (FV1000MPE, Olympus, Tokyo, Japan) (Figure 1C). Dextran-conjugated Texas Red (10 kDa MW; Invitrogen, Burlington, ON, Canada) was injected through the tail vein catheter for visualization of the vessels and dye leakage following the disruption of BBB. Ultrasound exposure and two-photon imaging were performed simultaneously. The blood vessels in the brain were illuminated with a mode-locked Ti: Sapphire laser unit set at 810 nm (Mai-Tai, Spectra-Physics, Irvine, CA, USA), which produced pulses with a repetition rate of 80 MHz. A $\times$ 25 water-immersion objective lens (1.05 NA, Olympus) was used. A stack of 10 images spanning 100 to 300 μm below cortical surface was acquired every 15 to 30 seconds.

Image Processing and Statistical Analysis

Images were processed with Olympus FluoView (FV1000, Olympus, 2009), ImageJ (Bethesda, MA, USA), and Matlab (The Mathworks, Natick, MA, USA). All images were converted to eight-bit grayscale before analysis. Regions of interest were demarcated along the vascular wall outside of the lumen to explore leakage of the dye by analyzing the intensity change over time. Peak time was recorded for each leaky vessel, which we arbitrarily set as time it took to reach 80% of maximum intensity. The reason for choosing 80% instead of maximum intensity was due to the nature of sustained leakage, which reaches plateau, making it hard for consistent measurement of peak time as we are trying to show the difference in all three types. By choosing 80%

instead of 100% of maximum intensity, we were able to differentiate the three leakage types not only graphically, but also numerically, especially between sustained and slow. The intraluminal diameters of the vessels were estimated by taking the full width at half maximum of the signal profile taken perpendicular to the local tangent to the vessels of interest. Statistical differences among the different leakage mechanisms were evaluated with one-way ANOVA followed by Newman–Keuls Multiple Comparison Test. A value of $P<0.05$ was considered as significant in all our analyses.

Results

In the controls, we observed no change in extravascular signal intensity with either MB injection or US exposure alone. The treated animals had distinct responses to MB/US treatment by displaying dye leakage compared with no leakage observed in the controls ($n=4$). In addition, treated animals that received MB injection 10 seconds before US sonication ($n=8$) did not show different results from those that received MB 10 seconds after the start of US sonication ($n=12$). The two different MB injection times resulted in about equal number of leaky vessels observed after US sonication; 22 vessels from eight animals that received MB injection before US sonication, and 30 vessels from 12 animals that were sonicated before MB injection. Among the 22 vessels from the first group, there were 16 vessels that displayed fast leakage, three sustained, and three slow. For the second group, out of the 30 leaky vessels, there were 18 fast leakage, four sustained, and eight slow. Of the 52 vessels from which we observed leakages, 35 were under 25 μm in diameter (Figure 2). By observing dye injection, we were able to differentiate the types of vessels pretreatment for

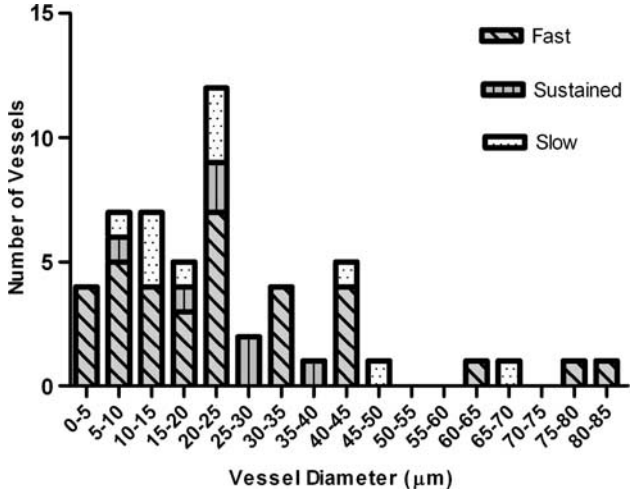

Figure 2 Size distribution of the vessels where leakage was observed. Vessel diameters were estimated by taking full width at half maximum of the signal intensity profile perpendicular to the local tangent.

13 vessels from five animals and we observed leakage from arteries (9/13) more often than veins (4/13).

Based on peak time for start of dye leakage, three types of leakage responses were identified (Figure 3A). The peak time for leakage significantly increased for slow leakage ($P<0.0001$) (Figure 3B). The first category, which we classified as fast leakage, was characterized by the detection of leakage within about a minute after the application of MB and US. The leakage appeared to be from point sources along the vessel wall (Figure 4A). The intensity decreased sharply with time after reaching the peak, dropping below 80% of the maximum intensity in 18 ± 3.6 seconds (mean $\pm$ s.d.). Second, sustained leakage was categorized as that which displayed a similar leakage response to the fast leakage, except that the peak intensity was maintained throughout the imaging session lasting up to an hour following cessation of sonication (Figure 4B). Finally, slow leakage was characterized by a longer time delay post-MB/US treatment until leakage was observed. In this case, leakage was observed along the entire length of the vessels instead of circulating from point sources (Figure 4C). Average peak time, which corresponded to reaching about 80% of peak intensity, was recorded for each leakage type (Table 1).

There was a correlation between leakage category and the observed vascular diameter (Figure 2). The fast leakage was observed from a wide range of vascular sizes, including the smallest to largest vessel size within our analyses. The sustained leakage included vessels of varying sizes similar to the fast leakage, but within a much smaller range of diameters. The sustained leakage comprised the highest median vessel diameter, but the upper limit on these vessel diameters was smaller than that of the vessels exhibiting fast leakage. It also had the smallest interquartile range. The slow leakage was observed mostly from smaller vessels under 25 μm in diameter, with the lowest median diameter of 15.2 μm among the three leakage types. Within the same animal, there were multiple leakages in a given FOV, most of which included capillary leakages on top of a few arterial and/or venous leakages. Capillaries responded immediately to MB/US treatment, constituting 37% of fast leakage.

Changes in acoustic pressures resulted in different leakage types. The higher the acoustic pressure, the more likely dye leakage started without delay upon the initiation of MB/US treatment (Figures 3B and 3C). The average negative acoustic pressure was lowest in the slow leakage type ($P=0.015$). The fast leakage occurred at all pressures used in our experiments (0.071 to 0.25 MPa). The sustained leakage also occurred from a wide range of acoustic pressures (0.071 to 0.13 MPa), but was more frequent in the low-to-intermediate range. Slow leakages resulted only from the lower acoustic pressures (0.071 to 0.10 MPa). The median negative peak pressure was the highest in fast leakage (0.13 MPa)

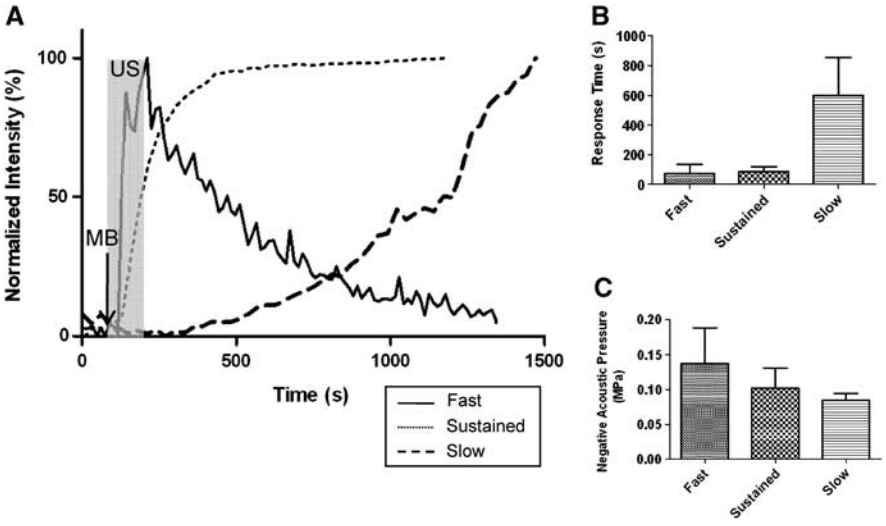

Figure 3 Three leakage types represented in plots. (**A**) Three types of leakage compared in leakage intensity curves. Ultrasound (US) sonication started at 90 seconds and ended at 210 seconds, indicated by the highlighted region. Microbubble (MB) bolus injection took place at 80 seconds. Fast leakage reached its peak soon after the sonication ended and the intensity decreased. Sustained leakage showed rapid increase in intensity during sonication period and maintained its high intensity throughout the imaging period. The vessels exhibiting slow leakage did not show changes for the first 10 to 20 minutes. (**B**) Comparison of average peak time of dye leakage for fast, sustained, and slow leakage. Significant differences are marked with asterisks. The level of significance was $P < 0.0001$. (**C**) Plot of negative acoustic pressure versus type of leakage. The fast leakage occurred at all levels of pressures, whereas the sustained and slow leakages usually occurred at low pressures. The level of significance was $P < 0.05$.

followed by sustained (0.10 MPa) and slow leakage (0.085 MPa) in decreasing order. The fast leakage was the most prevalent type among the three with the most number of vessels, 67% (35/52), displaying this type. Sustained leakage was observed from seven vessels and slow leakage from 11 vessels out of 52. There was no apparent correlation between acoustic pressure amplitude and diameter of the leaky vessels. All the pressures affected a wide range of vascular sizes. The highest pressure in the plot, 0.25 MPa, had the smallest mean diameter of leaky vessels.

Vessel caliber changes were not prevalent in most of the vessels we analyzed. About 25% (13/52) of the vessels constricted and 10% (5/52) dilated upon MB/US treatment, while the remaining 65% (34/52) showed no change in vessel diameter with leakage. Vasoconstriction and vasodilation were evident only in fast and sustained leakages, leaving the slow leakage free of changes in vessel diameter. Furthermore, there was an inverse correlation between the vessel size and the extent of constriction observed, with the percentage constriction decreasing with increasing vessel diameter (Figure 5A). The smallest vessel that constricted with the highest percentage of constriction in our data was 11.2 μm in diameter, excluding capillaries in vasoconstriction. As well, vasoconstriction occurred almost simultaneously with leakage in a number of cases. The combined plot of normalized intensity against the diameter of the vessel reveals that the increase in intensity correlates with the decrease in the size of intraluminal space (Figure 5B).

Brain tissues of those animals that displayed only one type of leakage were selected for histological analysis, two per each type (Figures 6A–6L). One of the two samples that were sonicated at low pressure (0.085 MPa) had small extravasations in the tissue, but not as extensive as the larger extravasations observed in the high-powered samples (Figures 6C and 6D). The petechiae were observed $\sim$400 μm away from the cortical surface of the animal. The other sample also sonicated at 0.085 MPa did not have any sign of extravasation. There was no apparent damage from the samples sonicated at 0.13 MPa (Figures 6E–6H). One of the samples sonicated at the high pressure (0.17 MPa) that displayed fast leakage from all leaky vessels had signs of extravasations of red blood cells near the site of sonication (Figures 6I and 6J).

Discussion

Vascular Size and Blood–Brain Barrier Disruption

Over 67% of the leaky vessels we analyzed were < 25 μm in diameter, the size that includes capillaries and smallest arterioles and venules (Burton, 1954). The high variability in the size of intraluminal space from 10's of μm to 100's μm across the vascular bed would have influenced MB–EC interactions inside the vessels. A much greater number of vessels underwent fast leakage (34/52) than sustained and slow leakages combined (18/52), because of the number of capillaries that were compromised

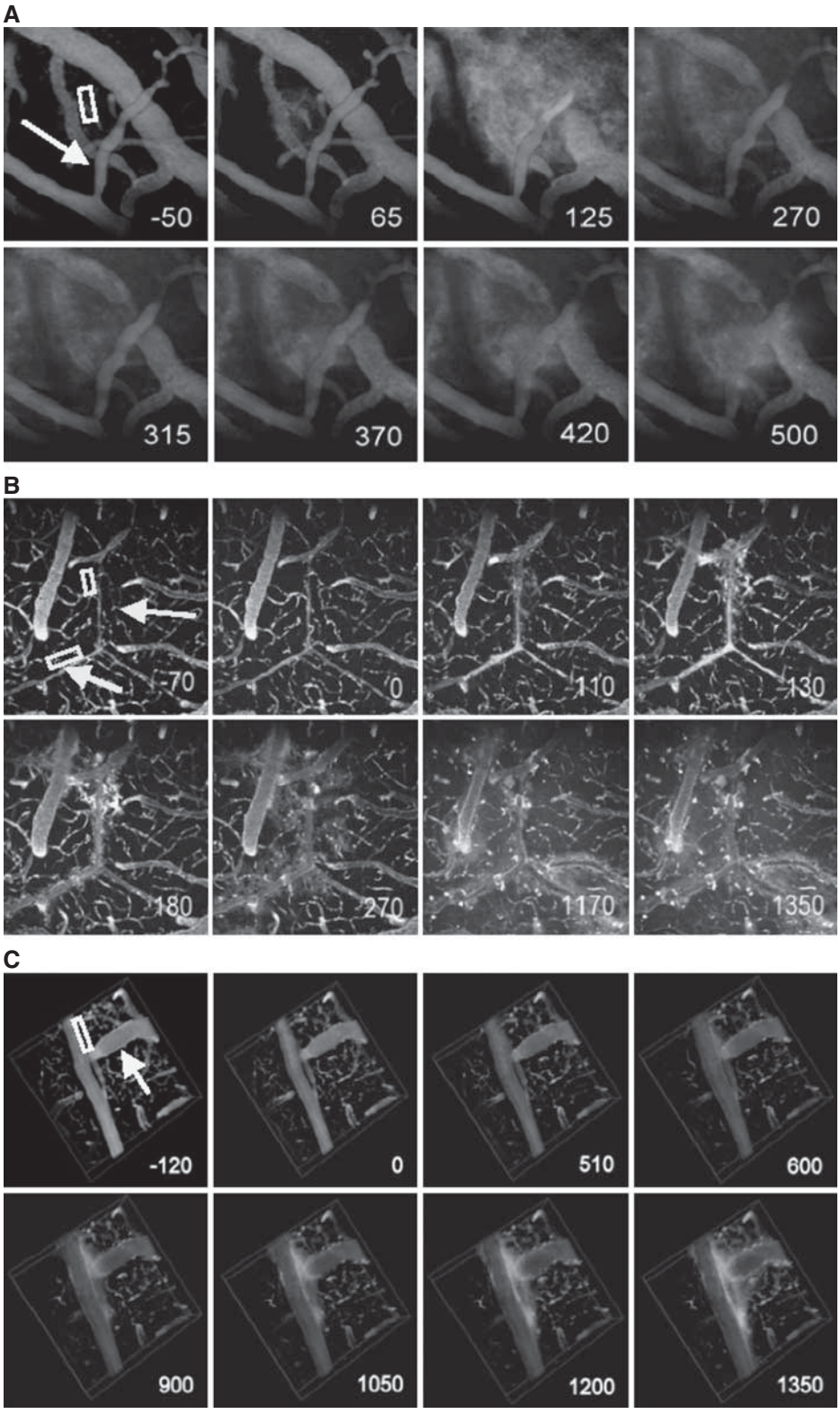

Figure 4 Three types of leakage represented in images acquired over time. The numbers in the bottom right corner indicate time (in seconds) from the start of ultrasound (US) sonication. US sonication ran from 0 to 120 seconds and microbubbles (MBs) were injected at 10 seconds. The regions of interest (ROIs) were indicated where signal intensity was measured over time. The arrow points to a vessel where vessel caliber change was observed. (**A**) *Z*-projection image ($512 \times 512\ \mu m^2$) of the vessels displaying a fast leakage. The negative acoustic pressure amplitude used here was 0.173 MPa. (**B**) *Z*-projection image ($512 \times 512\ \mu m^2$) of the vessels displaying a sustained leakage. $P = 0.13$ MPa. (**C**) 3D images ($512 \times 512 \times 100\ \mu m^3$) of the vessels displaying a slow leakage. $P = 0.0845$ MPa. No apparent leakage was observed until about 15 minutes after the start of US sonication.

Table 1 Summary of peak time from three leakage types in seconds

	Fast	*Sustained*	*Slow*
Average peak time (seconds)	73	84	602
s.d. (seconds)	61	34	253

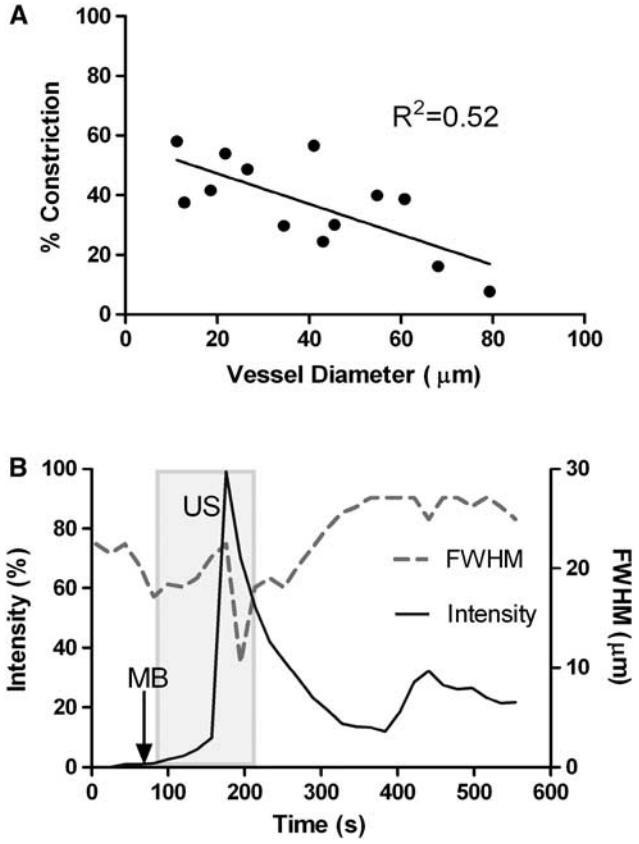

Figure 5 (**A**) Percentage constriction measured as a function of vessel diameter. For those vessels that have constricted during leakage, percentage constriction was taken by taking the minimum diameter observed over the course of time and the average diamater before ultrasound (US) sonication. (**B**) Vessel caliber change and leakage. Vasoconstriction occurred simultaneously with the rapid increase in extravascular regions of interest (ROI) signal intensity. US sonication started at 90 seconds and ended at 210 seconds. microbubbles (MBs) were injected at 100 seconds. FWHM, full width at half maximum.

immediately upon sonication. Since there is only a single layer of ECs that make up the capillary walls, capillaries would be more prone to fast disruption than bigger vessels, which have multiple cellular layers. The mean size of Definity MB is 1.1 to 3.3 μm in diameter and can expand up to 20 μm (Lantheus Medical Imaging). However, since the MBs are injected intravenously, the capillary bed in the lungs will filter out all of the larger bubbles. In cases where these MBs were sonicated while circulating in the capillaries, the tight junctions of the capillaries would have been disrupted by the expanding and contracting MBs that stretch the vessel wall. It is possible that this would disrupt the integrity of the tight junctions of the BBB as has been observed with electron microscopy (Sheikov *et al*, 2008). Additional mechanisms for transendothelial transport of molecules identified by electron microscopy analyses of US-induced BBB modulation include transcytosis, cytoplasmic opening of EC, and injured endothelial lining (Sheikov *et al*, 2004, 2008).

Vessel Diameter Change

An increase in intraluminal stress is known to cause vasoconstriction (Bayliss, 1902). The MB/US treatment would have imposed such stresses along the walls, initiating cascade effects that ultimately cause vasoconstriction. It is also possible that vasoconstriction occurred as a homeostatic mechanism in response to the hemorrhagic damages observed in fast leakage. The effects of vessel spasm and hemorrhage in US-induced BBB opening have been discussed in one of the earlier studies with the aim of avoiding adverse effects of US sonication on the blood vessels (Hynynen *et al*, 1996). Unlike the previous study by Raymond *et al* (2007) in which vasospasm was observed in 14 out of 16 locations, only 25% (13/52) of the vessels we analyzed experienced vasoconstriction with leakage. The lack of vasoconstriction in our animals might be the product of differences between the physiology of rats and mice. Rats are known to have a diminished vasomotor excitability that would cause them to be less responsive to the same mechanical stress from MB/US treatment than mice (Ayata *et al*, 2004). The exposure system used by Raymond *et al* (2007) also exposed the whole depth of the brain to similar pressures, thus potentially resulting in remote vascular effects, whereas our system induced the highest acoustic pressures in the tissue volume close to the brain surface.

We also observed vascular dilation, although this accounted for only 10% (5/52) of the total number of vessels. The relationship between vasodilation and the permeability of the BBB has been analyzed previously with alternative approaches to opening of the BBB. Stimulation of the parasympathetic sphenopalatine ganglion causes vasodilation of the cerebral vessels in rats (Suzuki *et al*, 1990). Using this finding as the basis of their work, Yarnitsky's group stimulated the parasympathetic sphenopalatine ganglion and found temporary increase in the permeability of the BBB, confirmed by the entry of various macromolecules into the brain (Yarnitsky *et al*, 2004). Another group has made a connection between disintegration of tight junctions of the BBB and matrix metalloproteinases, inflammatory agents that are released by various stimuli in the brain (Gurney *et al*, 2006), which cause vasodilation of the vessels at the site of incipient inflammation (Pober and Cotran, 1990). Although we did not observe

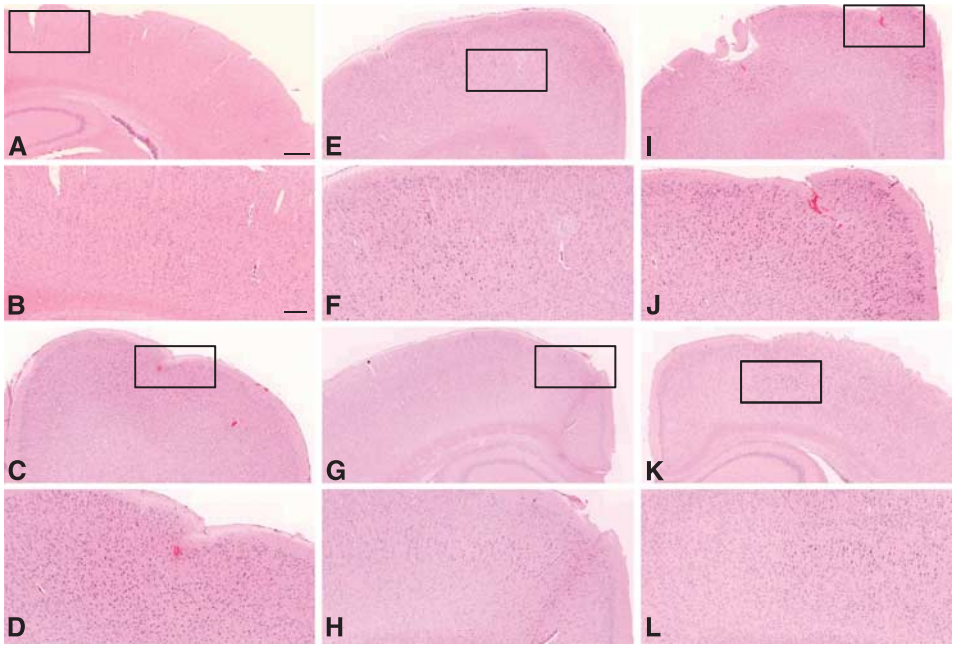

Figure 6 Histology evaluation of the brain tissues sonicated at varying acoustic pressures. The first and third rows of images are at $\times 5$ magnification and the second and the last rows are close-up images of the boxed regions at $\times 10$ magnification. Images (**A**–**D**) represent the low-power ultrasound treatment group (0.085 MPa). No extravasation of red blood cells was detected in sample (**A**), but some extravasation was observed in sample (**C**), as magnified in (**D**). Images (**E**–**H**) are from an intermediate treatment group (0.13 MPa) where there was no sign of damage. Images (**I**–**L**) are from a high-power treatment group (0.173 MPa). The sample (**I**) showed significant extravasation; however, the last set (**K**, **L**) showed no significant extravasation. The scale bar represents 500 μm for images at $\times 5$ and 200 μm for images at $\times 10$.

enough number of vasodilation to make it significant to altering the BBB permeability, it is possible that vasodilation and the BBB disruption are interrelated in the cerebral vasculature.

Vessel diameter changes that we observed in few cases could be further explained by the results of an *in vitro* study where microscopic images of MB–EC interactions were recorded with a fast framing camera (Van Wamel *et al*, 2004). The parameters of interest were crosssectional distance at two fixed points on an EC and MB diameter. In the study, there was an inverse relationship between the two variables observed over time: as the bubbles expanded, the membrane distance got shorter and as the bubbles shrank, the membranes separated apart from each other. The pushing and pulling of the cell membranes can be established by the dynamics of MB oscillation without cell lysis. Another study posits that shear stress caused by oscillating MBs likely modifies cellular permeability (Marmottant and Hilgenfeldt, 2003). The stretching of the capillaries due to expanding MBs has already been speculated as a possible mechanism for changing the permeability of the BBB (Hynynen *et al*, 2006). These vessel caliber changes can be indicative of the intraluminal stress that ultimately results in BBB disruption. All vessels that constricted leaked, but not all vessels that leaked constricted. Therefore, constriction is not essential to leakage, but it contributes to leakiness.

Venous Leakage

Another interesting observation noted from our study was leakage from the veins, which was not noted in previous studies of the BBB disruption. Veins are larger in diameter and have thinner and less rigid walls than arteries. In addition, the venous vasculature has a lower blood flow rate and fewer tight junctions that make the postcapillary venules the primary site of increased permeability during inflammation and prone to leukocyte trafficking (dela Paz and D'Amore, 2009). Thus, in addition to capillaries, which seemed to be the primary source of leakage in our data, the venules could also contribute to leakage.

Microbubble Injection Time

There was no significant difference among the results obtained from different MB injection times. Since there would have been more time for a thorough circulation of the MBs when injected before sonication, we anticipated more extensive leakage, especially from the capillaries. A study on Definity kinetics under therapeutic US conditions suggests that optimization of MB/US treatment requires a close monitoring on the kinetics of the MBs (Goertz *et al*, 2010). According to the study, efficiency of the MB/US treatment decreases if sonication burst occurs before the MBs fill up the

target area. We also expected that arteries would be more prone to leakage when MBs were injected after the start of the sonication since a bolus of MBs would be present only in the arteries for a brief time before circulating through the entire vasculature. Despite these speculations, we did not observe any notable change in the frequency or extent of leakage between the two MB injection trials. During the process of identifying vessel types through dye injection under continuous two-photon imaging, we observed that it took about up to 5 seconds for the dye to circulate throughout the cerebral vasculature. The half-life of Definity in blood is estimated to be 1.9 minutes (Lantheus Medical Imaging), which leaves more than a minute for MBs to be sonicated even if injected after US sonication has begun. Considering such fast circulation transit time, we speculate that there was not much difference resulting from MB injection time as long as MBs were under US exposure before they get eliminated in the circulation system. Previous studies on the BBB had a sonication period of less than a minute (Raymond *et al*, 2007; Hynynen *et al*, 2001, 2006). With our 120 seconds sonication period, the difference of 20 seconds in the duration of US sonication between the two different injection schemes did not result in distinguishable change.

Negative Acoustic Pressure Amplitudes

Variations in the interquartile, median, and mean negative peak pressure amplitudes among the three types of leakage reveal that peak negative acoustic pressures have influence over the leakage type (Figure 3C). Higher acoustic pressures would have caused bubble oscillation in greater amplitudes, transferring a strong mechanical stress on the tight junctions of the cells. On the other hand, MBs sonicated at lower pressures would not have imposed enough local force to immediately rupture the barrier. Although MBs vibrate in response to US pulses, they do not always make enough contact with the ECs to cause changes in the barrier integrity and permeability (Van Wamel *et al*, 2006). Our results can also be compared with the permeability study on the chorioallantoic membrane model with low-frequency contrast material-enhanced US (Stieger *et al*, 2007). Their study shows difference in the extent of enodothelial gaps and the mean velocity of extravasation flow of dextran between high mechanical stress and low-stress groups. Similar to our results where fast leakage had the highest mean negative acoustic pressure and slow leakage had the lowest mean (Figure 3C), both mean velocity and spatial gap were greater in high-stress group.

Leakage Types

For slow leakage, the response time varied in the range of 5 to 15 minutes until the intensity of the signal within the extravascular regions of interest started to change significantly. This time period is close to the duration of transcytosis of low-density lipoproteins taken across the ECs of the blood vessels, which was found to be about 15 minutes (Dehouck *et al*, 1997). We speculate that the mechanism responsible for initiating slow leakage is transcytosis, which does not occur in a normal BBB, but further investigation on the transcytotic activity across the ECs is necessary. The MB/US treatment increases both transjunctional and transcellular transfer of molecules from the lumen of the cerebral vessels into the interstitial space (Sheikov *et al*, 2004, 2006; Hynynen *et al*, 2005). The detailed analysis of the tight-junctional components after US sonication revealed the redistribution and diminished immunosignal detection of the proteins that maintain the barrier integrity, lasting up to 4 hours postsonication (Sheikov *et al*, 2008). Once disintegrated, molecular transfer would happen more prominently through transjunctional passage than transcellularly since transjunctional passage does not require energy expenditure. This is a possible explanation for the intensity curve for slow leakage, where initial increase in intensity corresponds to transcytotic transfer of dye followed by paracellular movement (Figure 3A).

One possibility for the cause of fast leakage comes from a puncture of the vessel wall that heals quickly. The signal intensity reduction is then caused by the diffusion of the dye into the surrounding tissues reducing the concentration in the regions of interest. It may be that the speed of the vessel wall repair is the major difference between the sustained and fast leakage. A study on cell sonoporation with MB/US treatment has shown temporary pore formation followed by quick resealing of cell membrane after sonication (Deng *et al*, 2004). The real-time measurement of the membrane potential shows that the transmembrane recovers to its original state following the US exposure, indication for resealing of the pores. With the pressure amplitude of <1 MPa and duration of 1 second of US sonication, the recovery time of sonoporation is found to be 4 to 10 seconds. Although the sonication parameters of that investigation are different from our experimental setup, the study reveals the possibility that pores are forming and instantly resealing, which would match the rapid increase to peak intensity and sharp decrease in intensity observed in fast leakage. Another explanation for reduction in intensity observed in fast leakage can be attributed to extravasations. A study on the millimolar absportivities of human hemoglobin in the visible and near-infrared spectra range reveals that their absorption peaks between 450 and 600 nm with the maximum near 554 nm (Zijlstra *et al*, 1991). The intensity curve could have decreased rapidly upon reaching the peak value due to the red blood cells leaking out of vessels. Extravasations have been also observed in previous studies on US-induced BBB opening (Hynynen *et al*, 2003; Liu *et al*, 2008). Although we observed in only

one out of the two samples that displayed fast leakage (Figures 6I and 6J), there has been evidence that results of inertial cavitation cause vessel rupture and provide passages for erythrocytes observed in the minor vascular damage (McDannold *et al*, 2007).

Understanding these different leakage types can have important roles to therapeutic studies using US/MB. The kinetics of the dye leakage can be further studied in pharmacokinetics. Applying knowledge of the intensity curve of the dye from our study, one could predict how therapeutic agents would be deposited in a targeted area over time. We have only used 10 kDa dextran-conjugated Texas Red for visualizing the vasculature and leakage from the BBB opening. In the previous two-photon study of the BBB opening 70 kDa Texas Red was used instead (Raymond *et al*, 2007), but they also observed different leakage mechanisms and their intensity curve showed rapid increase to peak during US sonication, similar to our fast and sustained leakage types. There could be fine differences in leakage mechanism arising from the difference in molecular weight of the fluorescent dye, but further study is needed to test the influence of the molecular weight in leakiness of the blood vessels.

Conclusions

In conclusion, we have found that different types of leakage can be attained by controlling peak negative pressure amplitude of sonication. The low powers seem to elicit transcytosis initially followed by formation of a transcellular gap that allows transport of materials from the lumen of the blood vessels into the intercellular space. The intermediate and high powers result in immediate response to MB/US treatment via multiple leakage patterns, resulting from a number of possible mechanisms, such as local puncture on the vascular wall and widening of the tight junctions. Vasoconstriction did not occur as frequently as we anticipated based on the previous multiphoton study of US-induced BBB opening. We observed some vasodilation in a small number of cases as well. The size of a blood vessel also influenced its response in terms of diameter changes and frequency of leakage: the smaller vessels are easier to disrupt even with low acoustic pressures. Our results show that US-induced BBB opening may potentially be more selective in vascular sizes and leakage mechanisms by controlling sonication pressure.

Acknowledgements

The authors thank Kun Zhang and Jianfei He for their technical assistance with animal care and the members of Focused Ultrasound Laboratory for their help in reviewing the manuscript.

Disclosure/conflict of interest

The authors declare no conflict of interest.

References

Ayata C, Shin HK, Salomone S, Ozdemir-Gursoy Y, Boas DA, Dunn AK, Moskowitz MA (2004) Pronounced hypoperfusion during spreading depression in mouse cortex. *J Cereb Blood Flow Metab* 24:1172–82

Bayliss WM (1902) On the local reactions of the arterial wall to changes of internal pressure. *J Physiol London* 28:220–31

Burton AC (1954) Relation of structure to function of the tissues of the wall of blood vessels. *Physiol Rev* 34:619–42

Choi JJ, Pernot M, Small SA, Konofagou EE (2007) Noninvasive, transcranial and localized opening of the blood-brain barrier using focused ultrasound in mice. *Ultrasound Med Biol* 33:95–104

Dehouck B, Fenart L, Dehouck MP, Pierce A, Torpier G, Cecchelli R (1997) A new function for the LDL receptor: transcytosis of LDL across the blood-brain barrier. *J Cell Biol* 138:877–89

dela Paz NG, D'Amore PA (2009) Arterial versus venous endothelial cells. *Cell Tissue Res* 335:5–16

Deng CX, Sieling F, Pan H, Cui JM (2004) Ultrasound-induced cell membrane porosity. *Ultrasound Med Biol* 30:519–26

Denk W, Strickler JH, Webb WW (1990) 2-photon laser scanning fluorescence microscopy. *Science* 248:73–6

Fenstermacher J, Kaye T (1988) Drug diffusion within the brain. In: *Annals of the New York Academy of Sciences* (Penn RD, ed), Vol 531. Neurological Applications of Implanted Drug Pumps; Conference, New York, NY, USA Illus: 1987 Ix+215p the New York Academy of Sciences: New York, NY, USA 29–39

Goertz DE, Wright C, Hynynen K (2010) Contrast agent kinetics in the rabbit brain during exposure to therapeutic ultrasound. *Ultrasound Med Biol* 36: 916–24

Gurney KJ, Estrada EY, Rosenberg GA (2006) Blood-brain barrier disruption by stromelysin-1 facilitates neutrophil infiltration in neuroinflammation. *Neurobiol Dis* 23:87–96

Howles GP, Bing KF, Qi Y, Rosenzweig SJ, Nightingale KR, Johnson GA (2010) Contrast-enhanced *in vivo* magnetic resonance microscopy of the mouse brain enabled by noninvasive opening of the blood-brain barrier with ultrasound. *Magn Reson Med* 64:995–1004

Hynynen K, Chung AH, Colucci V, Jolesz FA (1996) Potential adverse effects of high-intensity focused ultrasound exposure on blood vessels *in vivo*. *Ultrasound Med Biol* 22:193–201

Hynynen K, McDannold N, Sheikov NA, Jolesz FA, Vykhodtseva N (2005) Local and reversible blood-brain barrier disruption by noninvasive focused ultrasound at frequencies suitable for trans-skull sonications. *Neuroimage* 24:12–20

Hynynen K, McDannold N, Vykhodtseva N, Jolesz FA (2001) Noninvasive MR imaging-guided focal opening of the blood-brain barrier in rabbits. *Radiology* 220: 640–6

Hynynen K, McDannold N, Vykhodtseva N, Jolesz FA (2003) Non-invasive opening of BBB by focused ultrasound. *Acta Neurochir Suppl* 86:555–8

Hynynen K, McDannold N, Vykhodtseva N, Raymond S, Weissleder R, Jolesz FA, Sheikov N (2006) Focal disruption of the blood-brain barrier due to 260-kHz ultrasound bursts: a method for molecular imaging and targeted drug delivery. *J Neurosurg* 105:445–54

Jordao JF, Ayala-Grosso CA, Markham K, Huang YX, Chopra R, McLaurin J, Hynynen K, Aubert I (2010) Antibodies targeted to the brain with image-guided focused ultrasound reduces amyloid-beta plaque load in the TgCRND8 mouse model of Alzheimer's disease. *PLoS One* 5:1–8

Kinoshita M, McDannold N, Jolesz FA, Hynynen K (2006*a*) Noninvasive localized delivery of Herceptin to the mouse brain by MRI-guided focused ultrasound-induced blood-brain barrier disruption. *Proc Natl Acad Sci* 103:11719–23

Kinoshita M, McDannold N, Jolesz FA, Hynynen K (2006*b*) Targeted delivery of antibodies through the blood-brain barrier by MRI-guided focused ultrasound. *Biochem Biophys Res Commun* 340:1085–90

Kleinfeld D, Mitra PP, Helmchen F, Denk W (1998) Fluctuations and stimulus-induced changes in blood flow observed in individual capillaries in layers 2 through 4 of rat neocortex. *Proc Natl Acad Sci USA* 95:15741–6

Kobat D, Durst ME, Nishimura N, Wong AW, Schaffer CB, Xu C (2009) Deep tissue multiphoton microscopy using longer wavelength excitation. *Opt Express* 17:13354–64

Liu HL, Wai YY, Chen WS, Chen JC, Hsu PH, Wu XY, Huang WC, Yen TC, Wang JJ (2008) Hemorrhage detection during focused-ultrasound induced blood-brain-barrier opening by using susceptibility-weighted magnetic resonance imaging. *Ultrasound Med Biol* 34:598–606

Marmottant P, Hilgenfeldt S (2003) Controlled vesicle deformation and lysis by single oscillating bubbles. *Nature* 423:153–6

McDannold N, Vykhodtseva N, Hynynen K (2007) Use of ultrasound pulses combined with definity for targeted blood-brain barrier disruption: a feasibility study. *Ultrasound Med Biol* 33:584–90

McDannold N, Vykhodtseva N, Hynynen K (2008) Blood-brain barrier disruption induced by focused ultrasound and circulating preformed microbubbles appears to be characterized by the mechanical index. *Ultrasound Med Biol* 34:834–40

Oldendorf WH, Cornford ME, Brown WJ (1977) Large apparent work capability of blood-brain barrier-study of mitochondrial content of capillary endothelial cells in brain and other tissues of rat. *Ann Neurol* 1: 409–17

Pardridge WM (2005) The blood-brain barrier: bottleneck in brain drug development. *NeuroRx* 2:3–14

Pober JS, Cotran RS (1990) The role of endothelial-cells in inflammation. *Transplantation* 50:537–44

Raymond SB, Skoch J, Hynynen K, Bacskai BJ (2007) Multiphoton imaging of ultrasound/optison mediated cerebrovascular effects *in vivo*. *J Cereb Blood Flow Metab* 27:393–403

Raymond SB, Treat LH, Dewey JD, McDannold NJ, Hynynen K, Bacskai BJ (2008) Ultrasound enhanced delivery of molecular imaging and therapeutic agents in Alzheimer's disease mouse models. *PLoS One* 3:1–7

Reinhard M, Hetzel A, Kruger S, Kretzer S, Talazko J, Ziyeh S, Weber J, Els T (2006) Blood-brain barrier disruption by low-frequency ultrasound. *Stroke* 37:1546–8

Sedlakova R, Shivers RR, Del Maestro RF (1999) Ultrastructure of the blood-brain barrier in the rabbit. *J Submicrosc Cytol Pathol* 31:149–61

Sheikov N, McDannold N, Jolesz F, Zhang YZ, Tam K, Hynynen K (2006) Brain arterioles show more active vesicular transport of blood-borne tracer molecules than capillaries and venules after focused ultrasound-evoked opening of the blood-brain barrier. *Ultrasound Med Biol* 32:1399–409

Sheikov N, McDannold N, Sharma S, Hynynen K (2008) Effect of focused ultrasound applied with an ultrasound contrast agent on the tight junctional integrity of the brain microvascular endothelium. *Ultrasound Med Biol* 34:1093–104

Sheikov N, McDannold N, Vykhodtseva N, Jolesz F, Hynynen K (2004) Cellular mechanisms of the blood-brain barrier opening induced by ultrasound in presence of microbubbles. *Ultrasound Med Biol* 30: 979–89

Stieger SM, Caskey CF, Adamson RH, Qin SP, Curry FRE, Wisner ER, Ferrara KW (2007) Enhancement of vascular permeability with low-frequency contrast-enhanced ultrasound in the chorioallantoic membrane model. *Radiology* 243:112–21

Suzuki N, Hardebo JE, Skagerberg G, Owman C (1990) Central origins of preganglionic fibers to the sphenopalatine ganglion in the rat – a fluorescent retrograde tracer study with special reference to its relation to central catecholaminergic systems. *J Auton Nerv Syst* 30:101–9

Toole JF (1990) *Cerebrovascular Disorders*. In: Applied physiology of the cerebral circulation, 4th edn, New York, NY: Raven Press, 37–8

Van Wamel A, Bouakaz A, Versluis M, De Jong N (2004) Micromanipulation of endothelial cells: ultrasound-microbubble-cell interaction. *Ultrasound Med Biol* 30:1255–8

Van Wamel A, Kooiman K, Harteveld M, Emmer M, ten Cate FJ, Versluis M, de Jong N (2006) Vibrating microbubbles poking individual cells: drug transfer into cells via sonoporation. *J Control Release* 112:149–55

Yang FY, Fu WM, Yang RS, Lim HC, Kang KH, Lin WL (2007) Quantitative evaluation of focused ultrasound with a contrast agent on blood-brain barrier disruption. *Ultrasound Med Biol* 33:1421–7

Yarnitsky D, Gross Y, Lorian A, Shalev A, Lamensdorf I, Bornstein R, Shorer S, Mayevsky A, Patel KP, Abbott NJ, Mayhan WG (2004) Blood-brain barrier opened by stimulation of the parasympathetic sphenopalatine ganglion: a new method for macromolecule delivery to the brain. *J Neurosurg* 101:303–9

Zijlstra WG, Buursma A, Meeuwsenvanderroest WP (1991) Absorption-spectra of human fetal and adult oxyhemoglobin, de-oxyhemoglobin, carboxyhemoglobin, and methemoglobin. *Clin Chem* 37:1633–8